Suzuki, Y. Kojima, K. Nakajima, N. Kasai, T. Sakuma, Y. Kato, Y. Miyasaka, M. Yoshida, and S. Nishimoto, *Tech. Dig. Int. Electron Devices Meet.*, p. 675, IEEE (1996).
3. T. Kuroiwa, Y. Tsunemine, T. Horikawa, T. Makita, J. Tanimura, N. Mikami, and K. Sato, *Jpn. J. Appl. Phys.*, **33**, 5187 (1993).
4. H.-F. Chung, *J. Appl. Phys.*, **79**, 1965 (1996).
5. A. B. Catalan, J. V. Mantese, A. L. Micheli, N. W. Schubring, and R. J. Poisson, *J. Appl. Phys.*, **76**, 2541 (1994).
6. T. Kawahara, M. Yamamuka, T. Makita, K. Tsutahara, A. Yuuki, K. Ono, and Y. Matsui, *Jpn. J. Appl. Phys.*, **33**, 5897 (1994).
7. H. J. Cho, J. M. Lee, J. C. Shin, and H. J. Kim, *Integr. Ferroelectr.*, **14**, 115 (1997).
8. T. Kawahara, M. Yamamuka, A. Yuuki, and K. Ono, *Jpn. J. Appl. Phys.*, **34**, 5077 (1994).
9. C. S. Hwang, C. S. Kang, H.-J. Cho, S. O. Park, B. T. Lee, J. W. Kim, H. Horii, S. I. Lee, and M. Y. Lee, in Extended Abstracts of the Third Pacific Rim Conference on Ferroelectric Applications, p. 63 (1996).
10. S. Sone, H. Yabuta, Y. Kato, T. Iizuka, S. Yamamichi, H. Yamaguchi, P.-V. Lesaicherre, S. Nishimoto, and M. Yoshida, *Jpn. J. Appl. Phys.*, **35**, 5089 (1996).
11. C. S. Hwang, S. O. Park, H.-J. Cho, C. S. Kang, H.-K. Kang, S. I. Lee, and M. Y. Lee, *Appl. Phys. Lett.*, **67**, 2819 (1995).
12. S.-H. Paek, J. Won, K.-S. Lee, J-S. Choi, and C-S. Park, *Jpn. J. Appl. Phys.*, **35**, 5757 (1996).
13. P. Hesto, in *Instabilities in Silicon Devices: Silicon Passivation and Related Instabilities*, G. Barbottin and A. Vapaille, Editors, p. 263, Elsevier Science Publishers, North-Holland, Amsterdam (1986).

Electrical and Recombination Properties of Copper-Silicide Precipitates in Silicon

A. A. Istratov,[a,c] H. Hedemann,[b] M. Seibt,[b] O. F. Vyvenko,[b,c] W. Schröter,[b] T. Heiser,[a] C. Flink,[a] H. Hieslmair,[a] and E. R. Weber[a]

[a]*Department of Materials Science and Mineral Engineering, University of California, Berkeley, California 94720-1760, USA*
[b]*IV. Physical Institute, University of Göttingen, Göttingen D-37073, Germany*
[c]*Institute of Physics, St. Petersburg State University, St. Petersburg 198904, Russia*

ABSTRACT

Copper-silicide precipitates in silicon obtained after copper diffusion and quench in different liquids were studied by transmission electron microscopy and capacitance spectroscopy techniques. A correlation between the quenching rate, geometric size, and deep level spectra of the copper-silicide precipitates was established. The unusually wide deep level spectra are shown to be due to a defect-related band in the bandgap. The parameters of the band are evaluated using numerical simulations. A positive charge of copper-silicide precipitates in p-type and moderately doped n-type Si is predicted by simulations and confirmed by minority carrier transient spectroscopy measurements. Strong recombination activity of the precipitates due to attraction of minority carriers by the electric field around the precipitates and their recombination via the defect band is predicted and confirmed by the experiments. The pairing of copper with boron is shown to be an important factor determining the precipitation kinetics of the interstitial copper at room temperature.

In spite of its importance to the semiconductor industry, the electrical and structural properties of copper in silicon are poorly understood. At room temperature, most copper is found in precipitates and only a small fraction forms electrically or optically active point defects (in most cases less than 0.1% of the copper solubility, see Istratov and Weber[1] for a review). The size, density, and spatial distribution of copper precipitates are determined by the cooling rate, by the amount of copper present, and by the preexisting lattice defects. At relatively slow cooling rates, as obtained by air or furnace cooling, copper predominantly precipitates at wafer surfaces in the form of precipitate colonies,[2,3] whereas fast quenching (cooling rates >100 K/s) leads to the formation of precipitates of different morphologies in the bulk.[4,5]

As in the case of the other 3d transition metal impurities, undercooling of interstitially dissolved copper leads to a large chemical driving force Δf_C for precipitation[6] which is given by

$$\Delta f_C = k_B T \times \ln \frac{c}{c_{eq}} \quad [1]$$

where c is the actual impurity concentration and c_{eq} the concentration of the impurity at temperature T in equilibrium with the precipitating phase. More details of the physical meaning of the chemical precipitation driving force can be found in the literature on solid-state phase transformations (e.g., Ref. 7). For the case of the metal-silicide boundary phase, driving forces from several tenths of electron volts to several electron volts, depending on the undercooling, are readily estimated for all 3d transition metal impurities in silicon.

The precipitation behavior of metals is determined not only by chemical precipitation driving force, but also by their diffusivity. The 3d transition metals from Ti to Fe can be quenched interstitially and remain stable in this state since they become virtually immobile at low temperatures. Copper (like cobalt and nickel) features both a high chemical precipitation driving force and a high diffusivity even at room temperature. These factors lead to almost complete copper precipitation as the samples are cooled down.[8]

In this paper we report the results of studies of structural and electrical properties of copper-silicide precipitates in silicon.

Sample preparation for TEM and DLTS studies

For transmission electron microscopy (TEM) and deep level transient spectroscopy (DLTS) studies of copper-silicide precipitates, copper was diffused from a metal layer into (100)-oriented phosphorus-doped n-type float zone silicon samples. The free electron density, determined from capacitance-voltage characteristics (CV) at room temperature in as-grown samples, was 1.4×10^{15} cm^{-3}. Copper diffusion in a vertical furnace was followed by a quench in silicone oil, ethylene glycol, or 10% NaOH solution. The use of the vertical furnace enabled us to obtain better defined cooling procedures than the horizontal furnace used in the previous studies. Taking into account experimentally determined cooling rates for spherical silver samples,[9] and correcting for the different heat capacity of

Downloaded on 2016-05-09 to IP 130.203.136.75 address. Redistribution subject to ECS terms of use (see ecsdl.org/site/terms_use) unless CC License in place (see abstract).

silver and silicon and for the sample geometry, we estimated quenching rates of 200 K/s for silicone oil, 1000 K/s for ethylene glycol, and 2000 K/s for 10% NaOH. The diffusion temperature of 850°C, corresponding to the equilibrium copper solubility[10] of 10^{17} cm^{-3}, was chosen to obtain sufficient amplitude of the precipitate-related DLTS signal. As is shown below, even for this high Cu concentration, the density of precipitate-related deep levels did not exceed 10^{14} cm^{-3}. Consequently, no significant change of the free electron density was detected after the quench. Schottky diodes were fabricated by thermal evaporation of gold on chemically etched surfaces of n-type samples and of aluminum on p-type samples. Back-side ohmic contacts were prepared using GaAl eutectics.

TEM Studies of Copper-Silicide Precipitates after a Rapid Quench

TEM foils in (110) orientation were prepared from the bulk of the samples by standard techniques involving mechanical thinning followed by ion-milling. In order to avoid structural changes of the precipitates during sample preparation, we kept the temperature well below 100°C during thinning. For this, we used room temperature curing glues as well as liquid nitrogen cooling during ion

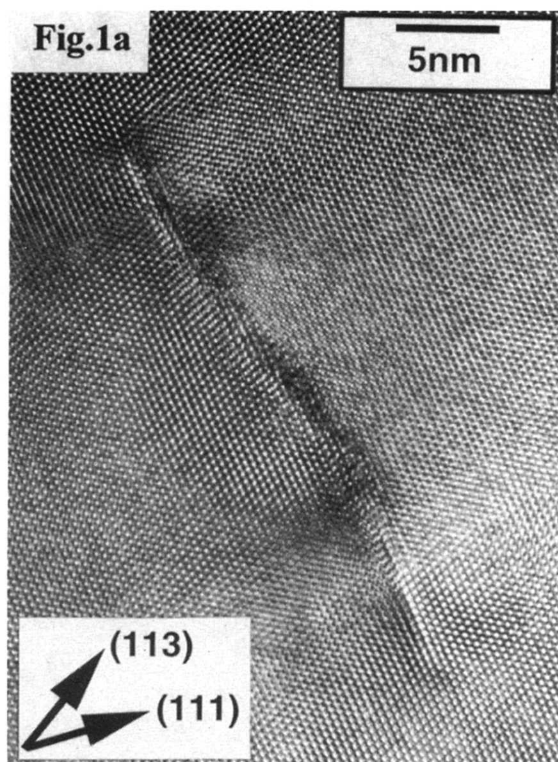

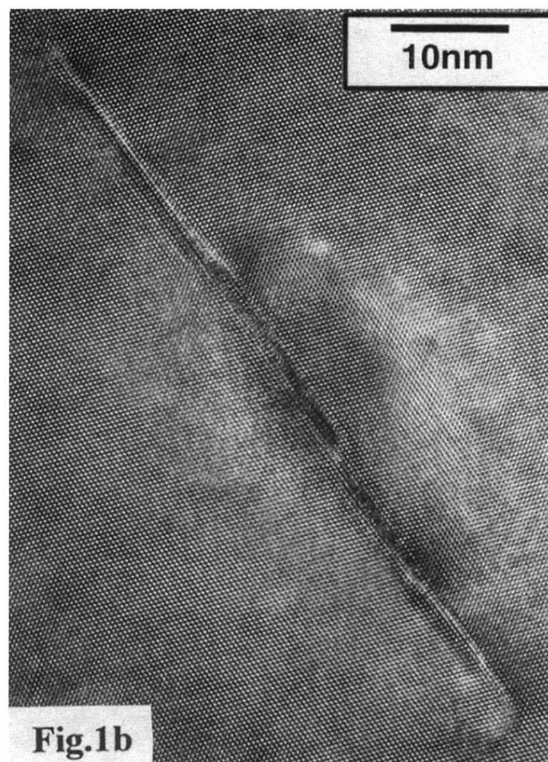

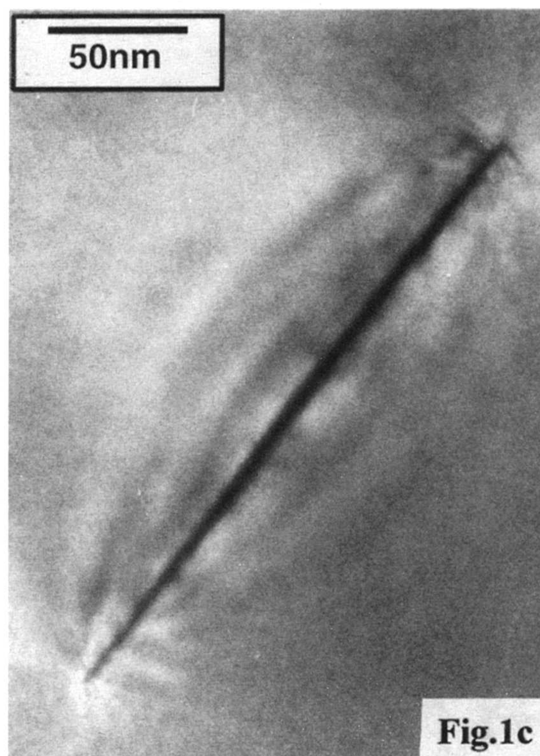

Fig. 1. TEM images of copper-silicide precipitates taken after copper diffusion at 850°C with subsequent quench in: (a) 10% NaOH solution (estimated cooling rate 2000 K/s), (b) ethylene glycol (estimated quenching rate 1000 K/s), (c) silicone oil (estimated cooling rate 200 K/s).

Downloaded on 2016-05-09 to IP 130.203.136.75 address. Redistribution subject to ECS terms of use (see ecsdl.org/site/terms_use) unless CC License in place (see abstract).

beam thinning which was done at an angle of 12°, an ion energy of 3 keV, and gun currents of 0.2 mA per gun using a GATAN DUO mill. Electron micrographs were obtained at 200 kV in a Philips CM200-UT-FEG.

TEM investigations in all cases revealed plate-shaped precipitates, mostly parallel to Si(111) planes as is shown in Fig. 1a-c. The highest cooling rate of approximately 2000 K/s leads to a high fraction of s-shaped precipitates (Fig. 1a) which besides the (111) habit plane show a (113) orientation in their central part. Platelets on Si(111) planes were observed for lower cooling rates. Figure 1b shows a plate-shaped precipitate obtained by quenching in ethylene glycol (estimated cooling rate: 1000 K/s) which consists of copper silicide in the central part and an extrinsic dislocation loop at the periphery. This can be seen more clearly in the high-resolution (HR) electron micrographs (Fig. 2). The copper silicide phase in Fig. 2a is revealed by the darker appearance of the central region which is restricted to two to three Si(111) layers and by additional reflections present in Fourier transforms of such lattice images. The extrinsic character of the dislocation loop is shown in Fig. 2b where the line indicates the rigid shift introduced in the silicon matrix by the precipitate. Quenching in silicone oil (200 K/s) produces larger precipitates with diameter of the order of 240 nm and thickness of about 5 nm which show no evidence for a surrounding extrinsic stacking fault (Fig. 1c). These precipitates are comparable with those reported in (Ref. 11). Strong lattice strains due to large volume expansion during the formation of copper silicide (the unit cell volume of Cu_3Si is 46 A^3 as compared to the molecular volume of silicon of 20 A^3 [12]) can be seen as contrasts around the precipitates in Fig. 1b and c.

Compared to previous work on the early stages of copper precipitation in silicon we have observed precursor stages (Fig. 1a, b and Fig. 2) to the plate-shaped copper silicide precipitates surrounded by extrinsic stacking faults as described previously.[4,5] Although the atomic structure of the very early stages is unknown, it is interesting to note the formation of defects with portions of Si(113) planes. Defects with (113) habit planes are also observed during the precipitation of oxygen and the agglomeration of self-interstitials.[13] The common feature of all three processes is the precipitation of interstitial atoms accompanied by a volume expansion. Hence, one might speculate that similar underlying physics leads to the formation of copper-silicide precipitates with (113) habit planes.

DLTS spectra of Copper-Silicide Precipitates Obtained Using Different Quenching Liquids and Their Comparison with Simulations.

DLTS spectra obtained on Cu-diffused samples after quenching in NaOH consist of a single peak of an unusual, almost rectangular shape (Fig. 3). DLTS measurements using different correlation frequencies revealed that the peak shifts along the temperature axis as a whole (Fig. 3b). No change in its shape was detected as would be expected if the peak were due to a superposition of independent point defects. Hence, we conclude that the peak stems from one single defect. Spectra obtained for different pulse widths (Fig. 3a) demonstrated a nonexponential capture behavior also pointing to an extended defect as a source of the spectra. Neither the shape of the spectra nor the capture kinetics could be satisfactorily explained by a simple Gaussian distribution of point defect levels as was proposed in the model of Omling et al.[14] It follows from Fig. 3, that the shape and temperature position of the high-temperature side of the peak is independent of the DLTS filling pulse width, whereas the low-temperature side changes as the pulse width increases. It has been recently shown by simulations[15,16] and analytical calculations,[17,18] that this kind of behavior is a fingerprint of bandlike states.

Unlike point defects, extended defects provide a distribution of states with different levels in the bandgap. Considering the electron exchange between these levels, extended defects may be classified into two groups depending on whether the exchange of electrons between the levels is fast or slow compared to the exchange with the bands of the host material.[15] In other words, the extended defect is

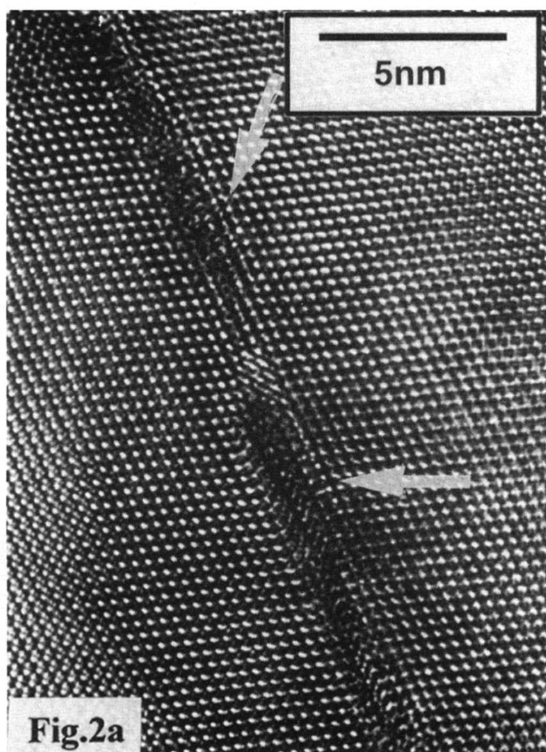

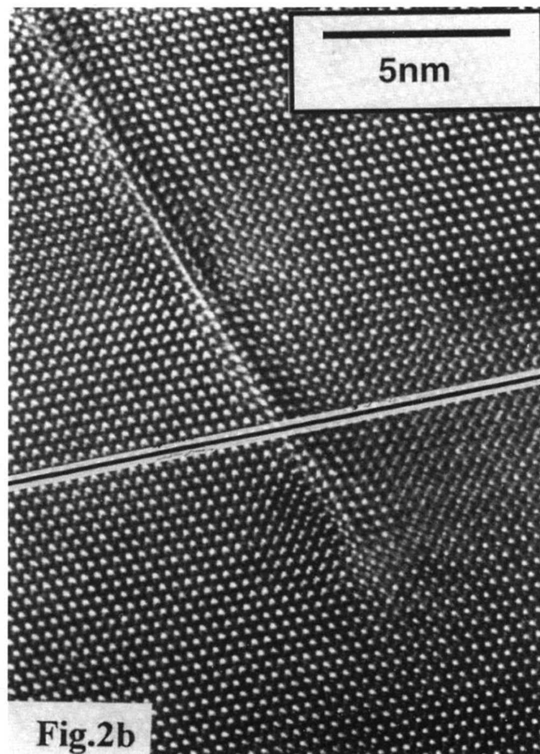

Fig. 2. Copper silicide precipitates after quenching in ethylene glycol: (a) HRTEM image of the central part of a copper-silicide platelet, the darker appearance as well as additional reflections in Fourier transforms of lattice image reveal the silicide phase; (b) shift of the silicon lattice planes on the opposite sides of the platelet, which gives evidence of the existence of an extrinsic dislocation loop surrounding the platelet.

Downloaded on 2016-05-09 to IP 130.203.136.75 address. Redistribution subject to ECS terms of use (see ecsdl.org/site/terms_use) unless CC License in place (see abstract).

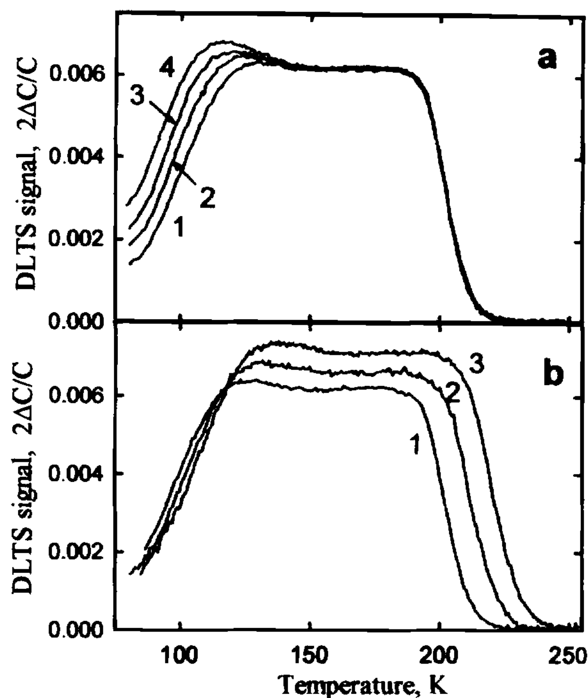

Fig. 3. Experimental DLTS spectra of the copper-silicide precipitates obtained after a fast quench of n-type silicon samples: (a) filling pulse width variation, t_p = 30 μs (curve 1), 300 μs (curve 2), 3 ms (curve 3), and 30 ms (curve 4); the spectra were taken with the sinusoidal lock-in correlation frequency f = 1.907 Hz. (b) Sinusoidal lock-in correlation frequency variation: curve 1, 1.907 Hz, curve 2, 7.63 Hz, curve 3, 30.52 Hz; filling pulse width t_p = 100 μs.

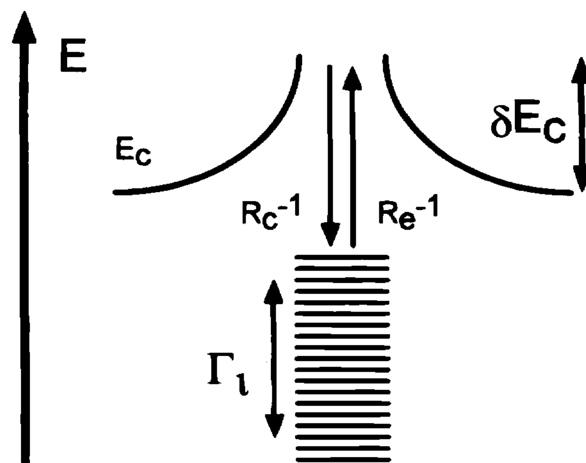

Fig. 4. Simplified band diagram of an extended defect constituted of an assembly of singles states in the bandgap. E_C is the conduction bandedge, δE_C is the band bending due to the common capture barrier; Γ_i is the internal equilibration time, and R_e^{-1}, R_c^{-1} are the inverse rates of emission and capture of carriers, respectively.

characterized by a certain internal equilibration time Γ_i which has to be compared with the inverse rates of capture R_C^{-1} and emission R_e^{-1} of free carriers (Fig. 4). If the internal equilibration time is much larger than the capture/emission time constants, the states of the extended defect are called "localized states." The emission from these states can be described as that of independent point defects while the capture is coupled due to a common capture barrier, which occurs when the sites of the states are close enough to form a superposed common coulomb field when charged. On the other hand, if the internal equilibration time is much smaller than the time constant of the carrier exchange with the bands, the defects are called "bandlike states." In this case, the extended defect may be considered as a conductor which provides a band of states within the bandgap of the host semiconductor. The occupancy of this band of defect states in the DLTS experiment is described by a quasi-Fermi distribution.

In the first study of bandlike states[15] it was assumed that the precipitates were neutral when empty and became negative when filled with electrons, i.e., that the precipitates created acceptorlike states in the bandgap. However, the quantitative description of spectra obtained from nickel-silicide precipitates was successful only when the defects were assumed amphoteric, i.e., the defect occupation $F^{(N)}$ when it is neutral was set to a nonzero value.[19] The capture barrier is given in this case by $\delta E = \alpha \times (F - F^{(N)})$ (see Fig. 4). For $NiSi_2$ precipitates $F^{(N)}$ was found to be between 0.3 to 0.5. Simulations with qualitative agreement with the DLTS data for copper silicide precipitates in n-type material (Fig. 3) have only been reached with $F^{(N)}$ = 0.8 to 1.0.

The simulated spectra are presented in Fig. 5. The simulation procedure is described in detail elsewhere.[17,18] The position of the defect band assumed for the simulations was between E_C − 0.15 eV and E_C − 0.35 eV. The shape of the peaks and their dependence on the correlation frequencies and pulse width reproduce the main features of the experimental curves. There remains, however, some difference in the slope of the low-temperature part of the spectra. Simulations predict a steeper slope of the low-temperature side than was found in the experiment. The possible nature of this discrepancy between the theory and the experiments is discussed below. The exact parameters of the defect band can be established only from numerical fits to the experimental spectra, where the above mentioned problem with the slope of the low T sides will be overcome. Such a fit requires an enormous amount of involved calculations (about 10^9 nonlinear rate equations have to be solved) and could not be accomplished at the time when the paper was prepared.

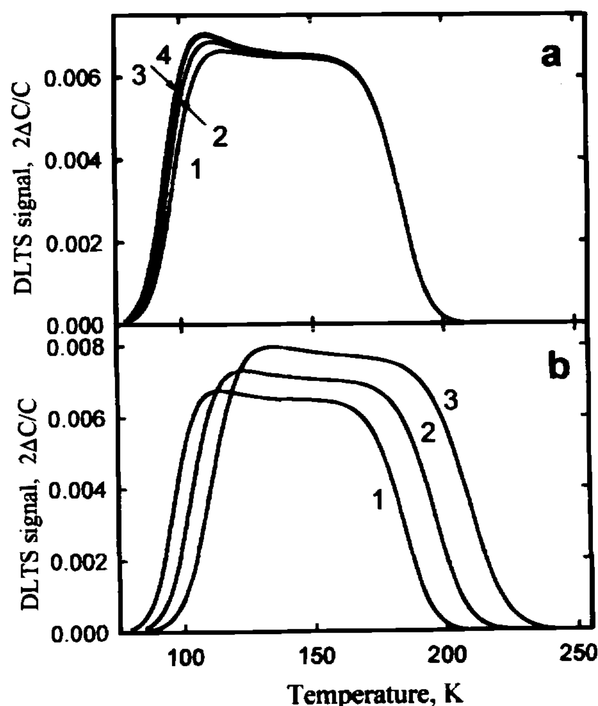

Fig. 5. Simulated pulse width and correlation frequency variations for a bandlike defect with a box-like distribution of levels between E_C − 0.15 eV and E_C − 0.35 eV, F_N = 0.91, α = 0.53 eV, capture cross section $\sigma = 1.0 \times 10^{-17}$ cm^{-2}, and a total concentration of deep levels of 2.0×10^{14} cm^{-3}. Further values of parameters are assumed as in the experimental spectra in Fig. 3.

Downloaded on 2016-05-09 to IP 130.203.136.75 address. Redistribution subject to ECS terms of use (see ecsdl.org/site/terms_use) unless CC License in place (see abstract).

Our experiments revealed a drastic dependence of the width, shape, and amplitude of the DLTS peak on the quenching rate. Typical DLTS spectra, obtained after copper diffusion at 850°C and subsequent quench in NaOH, ethylene glycol, and silicone oil are presented in Fig. 6. The spectra in Fig. 6 are normalized and should be used to compare widths of the DLTS peaks only, but not their relative amplitudes. The DLTS spectrum of the NaOH-quenched sample (cooling rate 2000 K/s) has an almost rectangular form with a width of about 100 K. A decrease of the cooling rate by a factor of two (ethylene glycol) resulted in a narrower peak with a width of about 70 K. Finally, a further fivefold decrease of the quenching rate led to a decrease of the peak width to one of only about 5 K larger than that of a point defect. As follows from Fig. 6, the high-temperature sides of the DLTS spectra for the samples quenched in ethylene glycol and silicone oil coincide while the high-temperature side of the spectrum obtained from the NaOH quenched sample is shifted by about 20 K toward higher temperatures. The experience of band structure calculations of extended defects such as stacking faults, grain boundaries, or dislocations suggests that the defect band of precipitates with a given structure does not change with size within the range of precipitate diameters obtained in this work. This means that precipitates with different sizes but the same structure should differ electrically mainly by the common capture barrier and the number of states. On the other hand, from analytical considerations about the DLTS spectra for bandlike states[17,18] it is known that the high-temperature sides of spectra for different pulse length are not affected by the common capture barrier. In other words, a scatter in the precipitate size and therefore the common capture barrier would change mainly the low-temperature side of DLTS lines. This agrees with the experimental findings. Comparing the spectra for the NaOH and the ethylene glycol quenched samples we conclude from the change in the high-temperature sides of the lines that there must be a quantitative change in the structure of the precipitates of the two samples and not only a difference in size. Some indications in favor of this conclusion follow from the TEM observations described in the preceding section.

DLTS spectra obtained after a silicone oil quench consisted of a relatively narrow DLTS peak with a peak amplitude corresponding to $N_T = 2.4 \times 10^{11}$ cm^{-3}. The peak was slightly wider than that of a point defect (Fig. 7), and the dependence of the peak amplitude on DLTS filling pulse width revealed a logarithmic capture kinetics (inset in Fig. 7), thus indicating that the peak is due to an extended defect. Although this peak is not a simple point defect, we made a conventional analysis by Arrhenius plot, which revealed the following apparent parameters of the center: an activation enthalpy of $E_a = 0.43$ eV and a capture cross section of $\sigma = 8 \times 10^{-14}$ cm^2 as obtained from the DLTS measurements with the filling pulse width of 100 μm. We call these values "apparent" since the parameters obtained for bandlike extended defects from an Arrhenius plot have been shown to be of no physical significance, because they depend strongly on the DLTS filling pulse width used in the measurements.[16] However, the Arrhenius plot may be seen as a condensed way of describing DLTS spectra, which is useful for comparison with published data which is generally confined to conventional analysis even for extended defects, provided all important parameters of the measurement are given. A copper-related DLTS peak with similar parameters was reported by Brotherton et al.[20] and Pearton et al.[21] The position of the peak (around 200 K in n-type silicon) is also close to the position of a broadened DLTS peak studied by Broniatowski et al.[22,23] Hamet et al.,[24] and Rizk et al.[25] However, due to the complex nature of the defects reported in Ref. 22-25 (copper-contaminated grain boundaries) a similar temperature position of the DLTS peaks is by no means sufficient to establish the identity of those defects with the defect states of the copper-silicide precipitates reported in this paper.

Observations of DLTS spectra of the copper precipitates in silicon obtained after a quench from a horizontal furnace have been reported in our recent paper.[5] The DLTS spectra reported in Ref. 5 seem similar to the ones obtained in this work for the samples quenched in silicone oil, although they are somewhat broader. It is possible that the samples[5] represent a state between the ones for our ethylene glycol and silicone oil quenched samples.

The charge state of Copper-Silicide Precipitates: MCTS Studies

Numerical simulations of the DLTS spectra of copper-silicide precipitates mentioned above showed that the precipitates form amphoteric bandlike states in the bandgap. The position of the defect band after a NaOH quench was

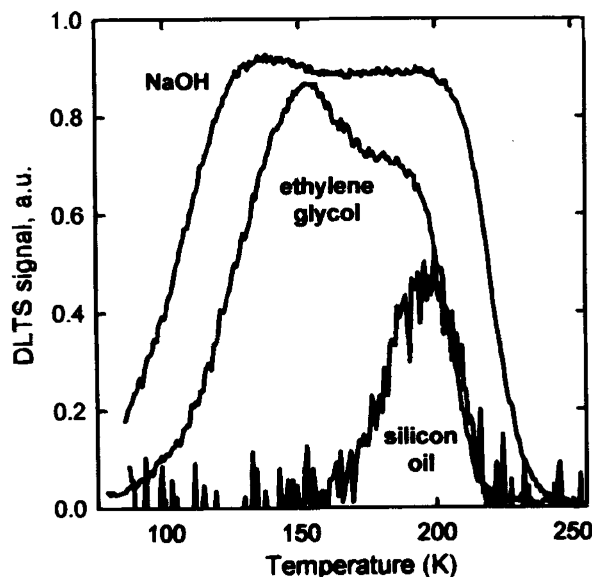

Fig. 6. Comparison of experimental DLTS spectra obtained on samples quenched in 10% NaOH, ethylene glycol, and silicone oil. The spectra were taken with the filling pulse duration t_p = 100 μs, DLTS correlation frequency f = 7.63 Hz.

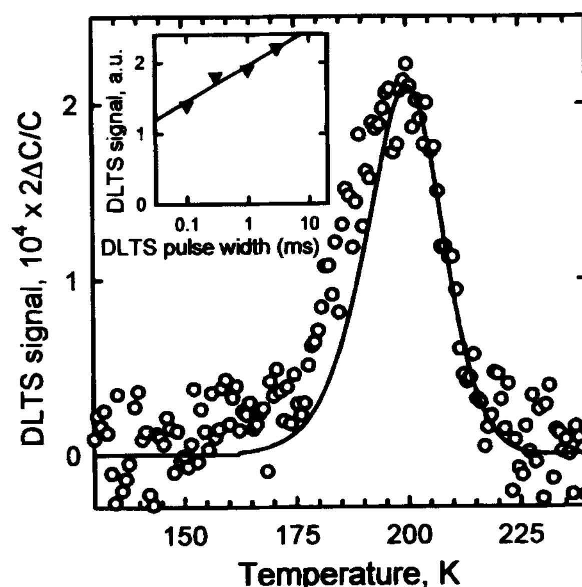

Fig. 7. An experimental DLTS peak obtained on the silicone oil-quenched sample (circles) and a simulated peak corresponding to a point defect (solid line) with the parameters obtained from the Arrhenius plot. The DLTS spectrum was taken with the bias voltage 3 V, filling pulse amplitude 2.8 V, filling pulse width 100 μs, sinusoidal lock-in correlation frequency 16 Hz. In the inset: capture kinetics of the defect (triangles) fits well into a logarithmic capture model.

Downloaded on 2016-05-09 to IP 130.203.136.75 address. Redistribution subject to ECS terms of use (see ecsdl.org/site/terms_use) unless CC License in place (see abstract).

estimated to be between $E_C - 0.15$ eV and $E_C - 0.40$ eV. The shape of the experimental DLTS spectra can be simulated only by assuming a high neutral occupation of the precipitates of approximately $F^{(N)} = 0.8$ to 1.0. This implies that the precipitates are neutral when the Fermi level lies at about $E_C - 0.20$ eV. In p-type silicon the precipitates should be positively charged at any temperature. In moderately doped n-type silicon they should be positively charged in the bulk of silicon at sufficiently high temperatures or in the depletion region (DR) of the Schottky diode, where the quasi-Fermi level lies below the neutral level of the precipitates. At lower temperatures the Fermi level should cross the neutral level and the precipitates will become neutral or negative in the bulk or in the DR just after application of the bias voltage drop pulse. Positively charged precipitates may be expected to attract electrons exhibiting an effective increase of the capture cross section for electrons, whereas a change of the charge state from positive to negative should result in formation of a repulsive potential, in substantial decrease of the electron capture cross section and in increase of the hole capture cross section.

To check the validity of this prediction, we have performed minority carrier transient spectroscopy (MCTS [26]) studies and compared three different modes of capacitance transient measurements: DLTS, MCTS, and DLTS/MCTS. MCTS is similar to DLTS except that the electrical filling pulses are substituted by light pulses. The DLTS/MCTS mode consists of a sequence of electrical and optical pulses. An optical pulse, following immediately after the electrical pulse, provides holes for capture and recombination with electrons, captured during the electrical pulse. The experimental spectra are presented in Fig. 8. Curve 1 is the conventional DLTS spectrum. Curve 2 was measured with a light pulse applied just after the voltage pulse (DLTS/MCTS mode). One can see that the illumination leads to a drastic decrease of the DLTS signal in a wide temperature interval and to the appearance of a negative signal at $T < 120$ K. Curve 3, measured when only light pulses were applied, mainly shows the same features as curve 2, but the sign of the signal changes at a higher temperature, i.e., at about 160 K. Note that at $T > 180$ K the signal amplitude of curve 3 becomes comparable to the conventional DLTS signal (curve 1) despite the much lower free electron density in the DR.

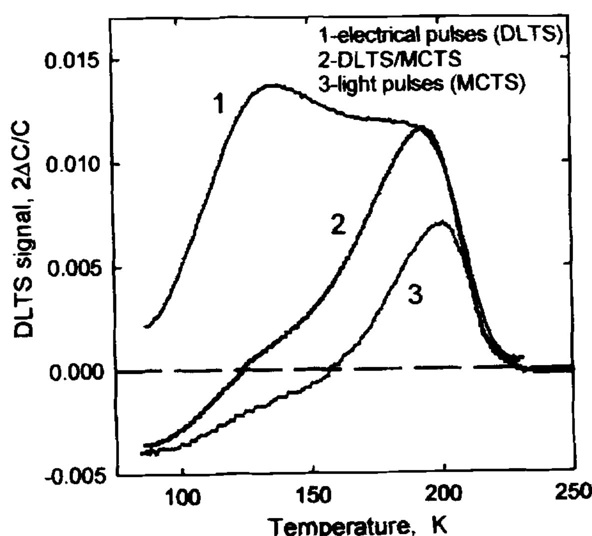

Fig. 8. DLTS and MCTS spectra of an n-type sample taken with the applied reverse bias voltage $U_{bias} = 5$ V. Copper diffusion at 850°C was terminated by quenching in NaOH. Curve 1, the voltage filling pules with the amplitude $V_p = U_{bias}$ (conventional DLTS), the duration $t_{vp} = 100$ µS; curve 2, the same electrical filling pulses following by the light pulses with the duration $t_{lp} = 100$ µS; curve 3, only light pulses with the duration $t_{lp} = 100$ µS (MCTS). Lock-in correlation frequency 64 Hz.

The exact interpretation of the MCTS and DLTS/MCTS spectra needs to be performed by numerical simulations and fits of the experimental spectra as described in the preceding section, including additionally the solution of the continuity equation within the DR under illumination. This procedure was too complex to be accomplished in this study. Instead, the apparent electron and hole capture cross section σ_n^{ap} and σ_p^{ap} were estimated at several characteristic temperature points by comparing the values of DLTS, MCTS, and DLTS/MCTS signals as measured using the same DLTS rate window and assuming a homogeneous space distribution of the excess carriers within the DR.

The estimates of ratios between the capture rates for the electrons and for the holes were calculated from the coincidence of DLTS and MCTS (or DLTS and DLTS/MCTS) signals and from the disappearance of MCTS-signal due to the electron emission from the traps. Omitting here and in the following the analysis of the rate equation, the first condition implies that the occupation of the precipitate electronic band states contributing to the electron emission within the used rate window is the same in both cases. The second condition implies that the states are empty.

The coincidence of DLTS and MCTS signals, observed at $T > 210$ K (Fig. 8), implies that the capture rate of holes during the light pulse is much lower than the capture rate of electrons: $c_n\Delta n >> c_p\Delta p$, where $c_n = \sigma_n^{ap}\langle\upsilon_n\rangle$ and $c_p = \sigma_p^{ap}\langle\upsilon_p\rangle$, where $\langle\upsilon_n\rangle$, $\langle\upsilon_p\rangle$ are the thermal velocity for the electrons and holes, respectively, σ_n^{ap} and σ_p^{ap} are the apparent capture cross sections for electrons and holes, and Δn, Δp are the nonequilibrium concentrations of electrons and holes generated in the DR by light.

In the DLTS/MCTS experiment, the electrical pulse fills the trap with electrons. The electron emission signal will disappear at $T < 130$ K if all electrons captured during the electrical pulse recombine with the holes. This occurs only if the defect states capture holes much faster during the light pulse than the electrons, i.e., $c_n\Delta n << c_p\Delta p$.

Finally, the last estimate can be done at $T \sim 190$ K, where the DLTS and DLTS/MCTS signal match. In this case, the defect occupation reached during the electrical pulse does not decrease during the subsequent light pulse. This is possible when the electron and hole capture rates during the light pulse are close to each other: $c_n\Delta n \sim c_p\Delta p$.

Hence, comparing the shape of the DLTS, DLTS/MCTS, and MCTS spectra, we established that the ratio of the electron and hole capture rates varies with the temperature: $c_n\Delta n << c_p\Delta p$ for $T \sim 130$ K, $c_n\Delta n \sim c_p\Delta p$ for $T \sim 190$ K and $c_n\Delta n >> c_p\Delta p$ for $T > 210$ K. The averaged absolute values of photogenerated holes Δp and electrons Δn within the DR were estimated using the results of recent calculations by Davidson et al.[27] from the measurements of the photocurrent flowing through the diode during the light pulse. In this way $\Delta n = 2 \times 10^8$ cm^{-3} and $\Delta p = 10^9$ cm^{-3} were derived. Since the density of light-injected electrons Δn and holes Δp in the DR differ only by a factor of five, the conditions derived above are defined mostly by the ratio of the apparent capture cross sections for electrons σ_n^{ap} and holes σ_p^{ap}.

A quantitative treatment of the electron and hole capture rates, based on the solution of the rate equation, while there was not enough room to include in this paper, enabled us to estimate the values of electron/hole capture cross sections at the three temperature points discussed above. The following estimates were obtained: $\sigma_p > 10^{-12}$ cm^{-2} at $T \sim 130$ K, $\sigma_p << 10^{-14}$ cm^{-2} at $T \sim 190$ K and $\sigma_n > 5 \times 10^{-12}$ cm^{-2} at $T > 210$ K.

The experimental results reported above agree well with the predictions of the simulations of DLTS spectra and indicate that the charge of copper-precipitates changes from negative to positive between temperatures 130 and 210 K. Note that this temperature range may vary for different quenching rates and different doping levels of the samples. A negative charge of copper-silicide precipitates at low temperatures explains the logarithmic dependence of the amplitude of the low temperature side of the copper precipitates-related DLTS-maximum on the filling pulse

Downloaded on 2016-05-09 to IP 130.203.136.75 address. Redistribution subject to ECS terms of use (see ecsdl.org/site/terms_use) unless CC License in place (see abstract).

duration (Fig. 3). The model of the logarithmic capture is well known and was successfully applied for electron capture by dislocations.[28]

Recombination Activity of the Precipitated Copper

The recombination activity of precipitated copper was studied comparing the minority carrier diffusion length of the samples, characterized by TEM and DLTS as above. The diffusion lengths of minority carriers, determined by EBIC from the dependence of collection efficiency vs. accelerating voltage,[29] are presented in Table I together with the value obtained earlier for the interstitial copper.[30]

As follows from Table I, copper-silicide precipitates are extremely active recombination centers. The diffusion length L_D in samples containing precipitated copper is only slightly larger than the average distance l between the precipitates. In contrast, the ratio L_D/l for the interstitial copper is about 1000. This means that the same concentration of copper is far more recombinative active when it is precipitated than when it is in the interstitial state, and that the recombination activity of copper-silicide precipitates cannot be obtained by just adding the recombination properties of single copper atoms. In our opinion, there are two mechanisms playing a decisive role in the recombination properties of copper-silicide precipitates. The first mechanism is the attraction of the charge carriers by space-charge regions around the precipitates. This model was suggested by Kittler et al.[31-33] to explain the unusually high recombination activity of nickel-silicide precipitates in silicon. The second important recombination mechanism is the recombination via the bandlike states of copper precipitates. As it follows from Shockley-Read-Hall statistics, the highest recombination activity is expected from defects which have a level close to the midgap. Copper-silicide precipitates form a defect band with a position quite close to the midgap. Therefore, the band can provide an excellent recombination channel for minority carriers, attracted by the electric field of charged precipitates.

The deleterious role of microdefects on the lifetime of minority carrier in solar cells has been discussed for a long time (see for example Ref. 34). It was suggested in Ref. 35 that intragranular defects in multicrystalline Si act as nucleation sites for metal contaminants (Cu, Fe, Co, Cr). Correia et al.[36] found that in Cu-contaminated samples the diffusion length of the minority carriers dropped by more than an order of magnitude due to defects in the form of platelets in (111) planes with a diameter of about 12 nm. These defects were surrounded by strong deformation fields, typical for Cu precipitates. This suggests that copper precipitates may be one of the defects responsible for the lifetime reduction in photovoltaic silicon.

As discussed above, the density of defect states can be determined only from an elaborate numerical fit, and the apparent defect density determined from the amplitude of the DLTS peak is much less than the real value. In our experiments, the samples quenched into 10% NaOH after 850°C anneal (equilibrium Cu solubility was about 10^{17} cm^{-3}) had a diffusion length less than 2 μm and the apparent amplitude of the DLTS signal was about $2\Delta C/C \sim 6 \times 10^{-3}$. If the density of precipitates decreased by a factor of 500, then the DLTS signal amplitude would drop below the detection limit ($2\Delta C/C \sim 10^{-5}$ for an average DLTS setup); however, using the Shockley-Read-Hall statistics, the diffusion length can be estimated to remain below 45 μm. This may explain why in PV silicon no deep levels in significant concentration have been found by DLTS in spite of the low minority carrier diffusion length.

Table I. Minority carrier diffusion length L_D, determined for the samples after different quench, and its ratio to the average distance between precipitates l, determined from the precipitates density N_p.

Type of recombination centers	N_p (cm^{-3})	l (μm)	L_d (μm)	Ratio L_d/l
NaOH, precipitates, n-Si, p-Si	4.3×10^{12}	0.6	<2.2	3.6
Ethylene glycol, precipitates, n-Si	1.1×10^{12}	1.0	<2.6	2.7
Silicone oil, precipitates n-Si	1.4×10^{9}	9	13	1.5
Interstitial copper, p-Si	10^{15}	0.1	110	1100

Precipitation Kinetics of the Interstitial Copper at Room Temperature

Until recently, little was known about the precipitation kinetics of the interstitial copper in silicon. Hall and Racette[37] were the first to show that copper diffuses in silicon predominantly in the interstitial state and that interstitial copper is a single donor. As far back as in 1954, they reported a metastable decrease of hole concentrations due to compensation by interstitial copper. Later, this phenomenon was studied by Prigge et al.[38,39] and by Zundel et al.[40] who introduced copper by chemomechanical polishing, and by Prescha et al.[41] and Wagner et al.[42] who diffused Cu at elevated temperatures. It was shown that copper can be quenched interstitially but is unstable at room temperature and precipitates in boron-doped Si within 10 to 15 h.[43]

Recent investigations revealed that interstitial copper precipitation has several unusual features which can be summarized as follows

1. In p-type silicon, one can quench copper interstitially in concentrations up to the doping level. As the diffusion temperature increases, the concentration of interstitially quenched copper follows the equilibrium copper solubility and saturates at a solubility close to the doping level.[43]
2. In n-type silicon, only very low concentrations of interstitial copper (in our experiments, about 10^{13} cm^{-3}) were detected in the interstitial state an hour after the quench.[44] Obviously, the concentration of copper dissolved during the diffusion anneal is determined solely by the diffusion temperature and does not depend on the conductivity type. This implies that the excess of copper above the doping level in p-Si or above approximately 10^{13} cm^{-3} in n-Si precipitates during the sample preparation, before the measurement begins.
3. Although interstitial copper is a donor, it is known from the literature (see Ref. 1 for a review), and confirmed by our experiments that the conductivity type of a sample cannot be inverted from p-type to n-type by Cu diffusion.

To establish the mechanism determining the Cu precipitation behavior, precipitation kinetics of copper were studied as a function of temperature in the range 270 to 333 K. The procedure used for sample preparation is described in the beginning of the article. Copper was diffused at 600°C, and the samples were quenched in ethylene glycol. Anneals at the indicated temperatures were made in a cryostat with zero bias voltage. The concentration of interstitial copper which is known to be a single donor,[37] was measured by capacitance-voltage characteristics (CV) at liquid nitrogen temperatures which prevented interstitial copper from drifting out of the depletion region during the CV measurement. The concentration of copper was determined by subtracting the apparent shallow acceptor concentration $N_a - N_{cu}$ from the concentration N_a when the copper precipitation is complete. One should note that the density of electrically active states of copper precipitates is several orders of magnitude lower than the copper concentration itself, and therefore the apparent change in the hole concentration results from only interstitial copper. The precipitation kinetics could be satisfactorily approximated by exponential decays. The dependence of the precipitation time constant in p-Si on inverse temperature is presented in Fig. 9. The data points on the plot could be interpolated by $\tau = 5.45 \times 10^{-6} \times \exp(0.55 \pm 0.05\ \mathrm{eV}/k_BT)$. Essentially the same dependence [$\tau = 1.10 \times 10^{-5} \times \exp(0.55 \pm 0.05\ \mathrm{eV}/k_BT)$] was obtained for n-type silicon,[44] although the interstitial copper concentration which could be detected was about two orders of magnitude less.

The meaning of the activation energy of 0.55 ± 0.05 eV is the height of a potential barrier which interstitial cop-

Downloaded on 2016-05-09 to IP 130.203.136.75 address. Redistribution subject to ECS terms of use (see ecsdl.org/site/terms_use) unless CC License in place (see abstract).

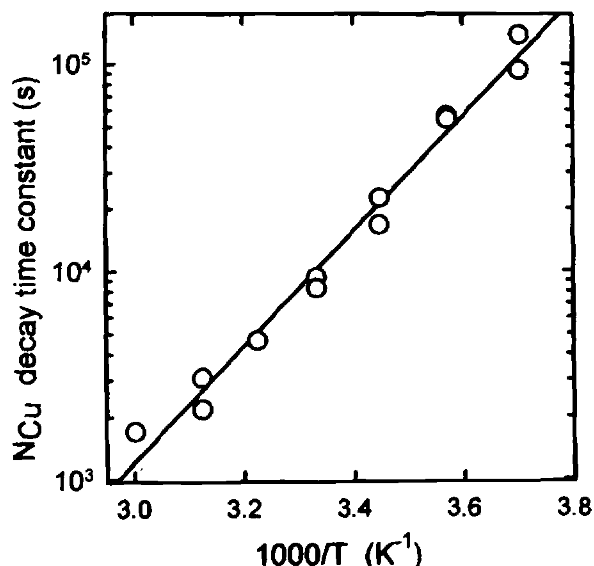

Fig. 9. Interstitial copper precipitation time constant measured in p-Si as a function of temperature.

per must overcome to precipitate. A certain activation energy for precipitation must exist since the precipitation process includes diffusion of metal atoms to the sinks. For example, the activation energy of iron precipitation was found[45] to be 0.70 ± 0.03 eV, which was in a good agreement with the diffusion enthalpy of interstitial Fe (0.68 eV).[10] Contrary to iron precipitation, the activation energy of copper precipitation (0.55 ± 0.05 eV) is higher than its experimentally measured diffusion enthalpy (0.43 eV as determined at high temperatures, and 0.39 eV as determined including the low-temperature data;[46] see also Note added in Proof at the end of the article.) This implies that there is another process besides the diffusion which limits the copper precipitation kinetics.

The value of 0.55 ± 0.05 eV is close to the binding energy of copper-boron pairs of 0.61 ± 0.02 eV.[41] However, the influence of copper-boron pairing on the effective diffusion coefficient of copper at room temperature was thought to be weak in the previous publications.[47] This conclusion was based on the theory of Reiss et al.,[48] who studied diffusion-limited capture of positively charged ions by immobile negatively charged acceptors. In their theory, the capture radius R_C is given by distance from the acceptor, on which the potential energy of coulomb attraction $V(r) = -q^2/4\pi\epsilon\epsilon_0 R$ exceeds the average thermal energy k_BT. The dissociation time constant of the inverse process, dissociation of Cu-acceptor pairs, can be determined experimentally and for CuB pairs is given by $\tau_e = 3.85 \times 10^{-14} \times \exp(0.61\ \text{eV}/k_BT)$.[41] The equilibrium fraction of copper paired with shallow acceptors is as follows[48]

$$\frac{N_{Cu}^{paired}}{N_{Cu}^{total}} = \frac{1}{2} \times \left(\alpha - \sqrt{\alpha^2 - 4N_a/N_{Cu}^{total}}\right) \qquad [2]$$

where

$$\alpha = 1 + \frac{N_a}{N_{Cu}^{total}} + \frac{\tau_c^0}{\tau_e \times N_{Cu}^{total}} \qquad [3]$$

τ_c^0 being $\tau_c \times (N_a - N_{cu}^{paired}) = (4\pi R_C D)^{-1}$. Using the copper diffusion coefficient of $D = 4.5 \times 10^{-3} \times \exp(-0.39\ \text{eV}/k_BT)$ from (Ref. 46), it is easily determined that, in boron doped silicon at room temperature, almost 90% of the total concentration of copper remains in the free interstitial state independent of the total concentration of copper in the sample. This implies that the dissociation of CuB pairs should not determine the copper precipitation rates at temperatures used in this study.

Since the experimental techniques which are used to detect interstitial copper concentration [CV, Hall effect, transient ion drift (TID)[49]] cannot distinguish unpaired interstitial copper from CuB pairs, the fraction of paired copper cannot be measured directly. However, one can evaluate a fraction of the unpaired copper from temperature-dependent TID measurements. According to the phenomenological model of transient ion drift,[49] the characteristic time constant of the capacitance transient due to copper drift out of the depletion region of a Schottky-diode is given by $\tau_{TID}^{-1} = (q^2N_A/\epsilon\epsilon_0 k_BT) \times D_{eff}$, where D_{eff} is the effective Cu diffusivity. In the case of strong Cu-acceptor pairing, the temperature dependence of the effective copper diffusivity is given by the dissociation energy of copper-acceptor pairs. On the other hand, a negligible copper-acceptor pairing results in D_{eff} equal to the copper diffusion coefficient.

The results of temperature-dependent TID measurements are presented in Fig. 10 for two types of samples: boron-doped and gallium-doped p-Si. In the case of the Ga-doped sample, the dependence has a slope equal to the dissociation energy of CuGa pairs in the whole temperature range from 295 to 375 K. This agrees with the expected from Reiss-Fuller theory strong (almost 100%) pairing of interstitial Cu with Ga. For boron-doped silicon, the dependence shows two linear parts with a bend at about $T = 330$ K. The slope of the dependence at $T > 330$ K can be satisfactorily described by a straight line with the slope of 0.38 eV, which is close to the Cu migration energy reported earlier,[49] whereas at $T < 330$ K the slope matches the dissociation energy of CuB pairs.[41] This indicates that in spite of the predictions of the Reiss-Fuller theory, CuB pairing is substantial at room temperature and can be neglected in Si:B, $[B] = 2 \times 10^{15}\ \text{cm}^{-3}$ only at $T > 330$ K. According to the recent results of exact numerical simulation of TID[50] the discrepancy is due primarily to some underestimation of the copper diffusivity determined from the phenomenological treatment in (Ref. 49).

An important conclusion of this experiment is that the copper precipitation kinetics in boron-doped silicon at room temperature is determined primarily by the diffusion of copper to the sinks. Because of the copper-boron pairing, the effective copper diffusion coefficient is at least several times lower than its value without pairing. Since the density of boron limits the concentration of copper which can form CuB pairs, the excess copper over the doping level does not pair with boron and precipitates quickly. This can explain why the maximum copper concentration which can be quenched interstitially is limited by the boron doping level. However, additional experiments are required to establish if the interaction between positively charged copper and positively charged copper precipitates may influ-

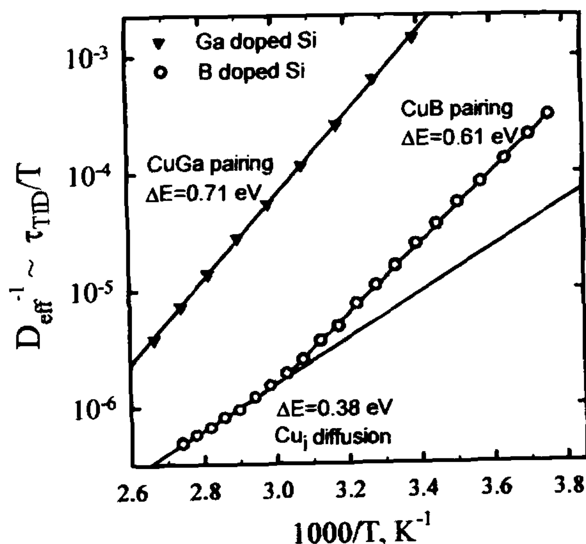

Fig. 10. Transient ion drift time constant as a function of temperature measured on boron-doped (open circles) and gallium-doped (triangles) samples.

Downloaded on 2016-05-09 to IP 130.203.136.75 address. Redistribution subject to ECS terms of use (see ecsdl.org/site/terms_use) unless CC License in place (see abstract).

ence the process of precipitate growth. The 10^{12} to 10^{13} cm^{-3} of interstitial copper detected in n-Si which decay with the same time constant as copper in p-Si are probably due to common and unintentional counterdoping of n-Si by boron. The surface contamination of silicon by boron at a level of up to 10^{13} cm^{-2} was detected by SIMS measurements[51] and has been shown to be of atmospheric origin.

Conclusions

It is shown that copper-silicide precipitates form bandlike states in the silicon bandgap. The defect band can be detected by DLTS. The shape of the DLTS peak correlates with the size of the precipitates, which is determined by the quenching rate. The model of the bandlike states enables one to explain the shape of the DLTS signal and its dependence on filling pulse width and DLTS rate window. The DLTS signal amplitude $2\Delta C/C$ substantially (up to several orders of magnitude) underestimates the density of defect states, which can be determined accurately only using numerical simulations. It is predicted by simulations and confirmed by MCTS measurements that the precipitates have amphoteric properties, i.e., they are positively charged at room temperature in p-Si and moderately doped n-Si and change their charge state to neutral or negative in n-Si as the sample is cooled down. Minority carrier lifetime measurements established very high recombination activity of the precipitates, which is explained by the attraction of charge carriers by space-charge regions around the precipitates and their recombination via the defect band. Studies of kinetics of interstitial copper precipitation revealed that the previous studies underestimated the pairing of copper with boron at room temperature. It is shown that trapping of copper by boron slows the precipitation rate to several hours at room temperature.

Acknowledgments

The authors are grateful to J. Weber for discussions on pairing of copper with acceptors, to W. Seifert, K. Knobloch, and M. Kittler for their help with the EBIC measurements, and to E. Edelson for this help with the preparation of the manuscript. The use of the Lawrence Berkeley National Laboratory experimental facilities which are funded through DOE is acknowledged. This work was partly supported by the National Renewable Energy Laboratory, WEDS, and Deutsche Forschungsgemeinschaft, Sonderforschungsbereich 345.

Manuscript received February 6, 1998. This was Paper 359 presented at the San Diego, California, Meeting of the Society, May 3-8, 1998.

The University of California, Berkeley, assisted in meeting the publication costs of this article.

Addendum: After this article was submitted, we made careful measurements of copper diffusivity in silicon at low temperatures. Using boron-doped silicon with a lower doping level than used here, we achieved the condition of weak pairing of interstitial copper with boron in a much wider temperature range than here (Fig. 10). This enabled us to determine the intrinsic diffusion barrier of copper in silicon; 0.18 ± 0.01 eV. Thus, the suggested hypothesis that the previous data substantially underestimated the diffusivity of copper at room temperature was confirmed experimentally. For a detailed description of the experiments see Ref. 52.

REFERENCES

1. A. A. Istratov and E. R. Weber, *Appl. Phys. A: Mater. Sci. Process*, **66**, 123 (1998).
2. E. Nes and J. Washburn, *J. Appl. Phys.*, **44**, 3682 (1973).
3. M. Seibt and K. Graff, *J. Appl. Phys.*, **63**, 4444 (1988).
4. M. Seibt, in *Semiconductor Silicon-1990*, H. R. Huff, K. G. Barraclough, and J.-I. Chikawa, Editors, PV 90-7, p. 663, The Electrochemical Society Proceedings Series, Pennington, NJ (1990).
5. M. Seibt, M. Grieβ, A. A. Istratov, H. Hedemann, A. Sattler, and W. Schröter, *Phys. Status. Solidi A*, **166**, 171 (1998).
6. W. Schröter, M. Seibt, and D. Gilles, in *Materials Science and Technology*, Vol. 4, R. W. Cahn, P. Haasen, and E. J. Kramer, Series Editors, W. Schröter, Editor, p. 539, VCH Weinheim (1991).
7. J. W. Christian, *The Theory of Transformations in Metals and Alloys: an Advanced Textbook in Physical Metallurgy*, Pergamon Press, Oxford (1965).
8. M. Seibt, in *Crystalline Defects and Contamination: Their Impact and Control in Device Manufacturing II*, B. O. Kolbesen, C. Clays, P. Stallhofer, and J. F. Tardiff, Editors, PV 97-22, p. 243, The Electrochemical Society Proceedings Series, Pennington, NJ (1997).
9. F. Eisenkolb, *Einführung in die Werkstoffkunde*, Vol. 3, p. 115, VEB Verlag Technik, Berlin (1961).
10. E. R. Weber, *Appl. Phys. A: Solids Surf.*, **30**, 1 (1983).
11. M. El Kajbaji and J. Thibault, *Philos. Mag. Lett.*, **71**, 335 (1995).
12. M. Ronay and R. G. Schad, *Phys. Rev. Lett.*, **64**, 2042 (1990).
13. A. Bourret, *Inst. Phys. Conf. Ser.*, **87**, 39 (1987).
14. P. Omling, E. R.Weber, L. Montelius, and H. Alexander, *Phys. Rev. B*, **32**, 6571, (1985).
15. W. Schröter, J. Kronewitz, U. Gnauert, F. Riedel, and M. Seibt, *Phys. Rev. B*, **52**, 13726 (1995).
16. H. Hedemann and W.Schröter, *J. Phys. III*, **7**, 1389 (1997).
17. H. Hedemann, Ph.D. Thesis, Cuvillier-Verlag Göttingen, ISBN 3-89588-377-8 (1995).
18. H. Hedemann and W. Schröter, *Phys. Rev. B*, Submitted.
19. F. Riedel, J. Kronewitz, U. Gnauert, M. Seibt, and W. Schröter, *Solid State Phenom.*, **47-48**, 359 (1995).
20. S. D. Brotherton, J. R. Ayres, A. Gill, H. W. van Kesteren, and F. J. A. M. Greidanus, *J. Appl. Phys.*, **62**, 1826 (1987).
21. S. J. Pearton and A. J.Tavendale, *J. Appl. Phys.*, **54**, 1375 (1983).
22. A. Broniatowski and C. Haut, *Philos. Mag. Lett.*, **62**, 407 (1990).
23. A. Broniatowski, *Phys. Rev. Lett.*, **62**, 3074 (1989).
24. J. F. Hamet, R. Abdelaoui, and G. Nouet, *J. Appl. Phys.*, **68**, 638 (1990).
25. R. Rizk, X. Portier, G. Allais, and G. Nouet, *J. Appl. Phys.*, **76**, 952 (1994).
26. R. Brunwin, B. Hamilton, P. Jordan and A. R. Peaker, *Electron. Lett.*, **15**, 349 (1979).
27. J. A. Davidson and J. H. Evans, *J. Appl. Phys.*, **81**, 251 (1997).
28. R. Labusch and W. Schröter, *Phys. Status Solidi*, **36**, 539 (1969).
29. A. A. Istratov, H. Hieslmair, T. Heiser, C. Flink, E. R. Weber, W. Seifert, and M. Kittler, in *VIIth Workshop on the Role of Impurities and Defects in Silicon Device Processing*, B. L. Sopori, Editor, p. 158, NREL, Golden, CO (1997).
30. A. A. Istratov, C. Flink, H. Hieslmair, T. Heiser, and E. R. Weber, *Appl. Phys. Lett.*, **71**, 2121 (1997).
31. M. Kittler, J. Lärz, W. Seifert, M. Seibt, and W. Schröter, *Appl. Phys. Lett.*, **58**, 911 (1991).
32. M. Kittler and W. Seifert, *Phys. Status Solidi A*, **150**, 463 (1995).
33. M. Kittler and W. Seifert, *Mater. Sci. Forum*, **196-201**, 1123 (1995).
34. J. Bailey and E. R.Weber, *Phys. Stat. Sol. A*, **137**, 515 (1993).
35. M. Werner, E. R. Weber, S. McHugo, and K. L. Chapman, *Solid State Phenom.*, **51-52**, 81 (1996).
36. A. Correia, D. Ballutaud, A. Boutry-Forveille, and J. L. Marice, *J. Appl. Phys.*, **78**, 6543 (1995).
37. R. N. Hall and J. H. Racette, *J. Appl. Phys.*, **35**, 379 (1964).
38. H. Prigge, P. Gerlach, P. O. Hahn, A. Schnegg, and H. Jacob, *J. Electrochem. Soc.*, **138**, 1385 (1991).
39. J. Hage, H. Prigge, and P. Wagner, *Appl. Phys. A: Solid Surf.*, **50**, 241 (1990).
40. T. Zundel, J. Weber, B. Benson, P. O. Hahn, A. Schnegg, and H. Prigge, *Appl. Phys. Lett.*, **53**, 1426 (1988).
41. Th. Prescha, T. Zundel, J. Weber, H. Prigge, and P. Gerlach, *Mater. Sci. Eng.*, **B4**, 79 (1989).
42. P. Wagner, H. Hage, H. Prigge, Th. Prescha, and J. Weber, in *Semiconductor Silicon-1990*, H. R. Huff, K. G. Barraclough, and J.-I. Chikawa, Editors, PV 90-7, p. 675, The Electrochemical Society Proceedings Series, Pennington, NJ (1990).
43. T. Heiser, S. A. McHugo, H. Hieslmair, and E. R. Weber, *Appl. Phys. Lett.*, **70**, 3576 (1997).
44. A. A. Istratov, H. Hieslmair, C. Flink, T. Heiser, and E. R. Weber, *Appl. Phys. Lett.*, **71**, 2349 (1997).

Downloaded on 2016-05-09 to IP 130.203.136.75 address. Redistribution subject to ECS terms of use (see ecsdl.org/site/terms_use) unless CC License in place (see abstract).

45. D. Gilles, E. R.Weber, and S. Hahn, *Phys. Rev. Lett.*, **64**, 196 (1990).
46. A. Mesli, T. Heiser and E. Mulheim, *Mater. Sci. Eng.*, **B25**, 141 (1994).
47. A. Zamouche, T. Heiser, and A. Mesli, *Appl. Phys. Lett.*, **66**, 631 (1995).
48. H. Reiss, C. S. Fuller, and F. J. Morin, *The Bell System Technical J.*, **35**, 535 (1956).
49. T. Heiser and A. Mesli, *Appl. Phys. A*, **57**, 325 (1993).
50. T. Heiser and E. R. Weber, *Phys. Rev. B*, **58**, 3893 (1998).
51. F. A. Stevie, E. P. Martin, Jr., P. M. Kahora, J. T. Cargo, A. K. Nanda, A. S. Harrus, A. J. Muller, and H. W. Krautter, *J. Vac. Sci. Technol.*, **A9**, 2813 (1991).
52. A. A. Istratov et al., *Phys. Rev. Lett.*, **81**, 1243 (1998)

Mechanism of Particle Growth of a $BaMgAl_{10}O_{17}:Eu^{2+}$ Phosphor by Firing with AlF_3

Shozo Oshio and Tomizo Matsuoka

Matsushita Electric Industrial Company, Limited, Lighting Research Laboratory, Kyoto 619-0237, Japan

Shosaku Tanaka and Hiroshi Kobayashi

Department of Electrical and Electronic Engineering, Tottori University, Tottori 680-0945, Japan

ABSTRACT

The mechanism of particle growth of the blue emitting $BaMgAl_{10}O_{17}:Eu^{2+}$ phosphor by firing with AlF_3 has been clarified. It was found that the reaction between $BaMgAl_{10}O_{17}:Eu^{2+}$ and AlF_3 during firing, on the basis of the following chemical equation, results in recreation of $BaMgAl_{10}O_{17}:Eu^{2+}$ with particle growth

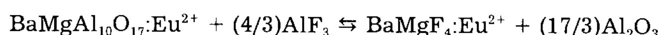

$$BaMgAl_{10}O_{17}:Eu^{2+} + (4/3)AlF_3 \leftrightharpoons BaMgF_4:Eu^{2+} + (17/3)Al_2O_3$$

the firing of $BaMgAl_{10}O_{17}:Eu^{2+}$ with AlF_3 first converts the phosphor into a mixture of the two compounds, $BaMgF_4:Eu^{2+}$ and Al_2O_3, at around 1200°C. The $BaMgF_4:Eu^{2+}$ melts at temperatures over 1000°C, then reacts with Al_2O_3, and participates in the recreation of both $BaMgAl_{10}O_{17}:Eu^{2+}$ and AlF_3 through a chemical reaction between the two compounds at 1200°C in $BaMgF_4:Eu^{2+}$ solutions. Recreated AlF_3 appears to sublime immediately because it is a material which sublimates with heating. This paper proposes a mechanism for the growth of particle of recreated $BaMgAl_{10}O_{17}:Eu^{2+}$ by the melting of $BaMgF_4:Eu^{2+}$.

Introduction

The efficient blue phosphor $BaMgAl_{10}O_{17}:Eu^{2+}$ has been applied to fluorescent lamps (FL) and plasma display panels (PDP) as a blue component.[1-6] $BaMgAl_{10}O_{17}:Eu^{2+}$ has conventionally been produced by the firing of the mixture of $BaCO_3$, basic $MgCO_3$, Al_2O_3, and Eu_2O_3 in a reducing atmosphere in the temperature range of 1200-1600°C.[7-9] In $BaMgAl_{10}O_{17}:Eu^{2+}$ production, AlF_3, which is a reactant added to the raw materials, has been extensively used to control the particle size of $BaMgAl_{10}O_{17}:Eu^{2+}$ in the range of 3-8 μm.[7,8] AlF_3 plays an important role in the particle growth of $BaMgAl_{10}O_{17}:Eu^{2+}$ and has been considered to act as a flux. However, there has been no detailed report on the function of AlF_3 in the mechanism of $BaMgAl_{10}O_{17}:Eu^{2-}$ particle growth.

In our experiment, such particle growth also occurs in a simple chemical reaction of $BaMgAl_{10}O_{17}:Eu^{2+}$ and AlF_3. Furthermore, it was found that products having particle growth following the chemical reaction of $BaMgAl_{10}O_{17}:Eu^{2+}$ and AlF_3 were almost always $BaMgAl_{10}O_{17}:Eu^{2+}$. To clarify the function of AlF_3 in the particle growth of $BaMgAl_{10}O_{17}:Eu^{2+}$, the chemical reaction of $BaMgAl_{10}O_{17}:Eu^{2+}$ and AlF_3 were studied in detail.

Experimental

In this study, $BaMgAl_{10}O_{17}:Eu^{2+}$ containing 10 atom % Eu^{2+} ions, that is the $Ba_{0.9}Eu_{0.1}MgAl_{10}O_{17}$ compound was used as the raw material. The $BaMgAl_{10}O_{17}:Eu^{2+}$ was prepared by firing a mixture consisting of $BaCO_3$, basic $MgCO_3$, Al_2O_3, and Eu_2O_3 in a reducing atmosphere of 95% nitrogen and 5% hydrogen at 1600°C for 2 h. To investigate the reaction of $BaMgAl_{10}O_{17}:Eu^{2+}$ and AlF_3, the effect of the amount of the reactant AlF_3 on particle size and the effect of firing temperature on particle size were studied. Particle sizes of these products was determined by scanning electron microscopy (SEM), and constituents of the products were examined by X-ray diffractometry (XRD). Photoluminescence spectra were also measured under ultraviolet light of 253.7 nm from a low-pressure mercury lamp to evaluate the products.

Results

Aspects of particle growth.—To confirm that particle growth occurred while maintaining the crystal structure of $BaMgAl_{10}O_{17}:Eu^{2+}$ through the simple chemical reaction of $BaMgAl_{10}O_{17}:Eu^{2+}$ and AlF_3, mixtures of $BaMgAl_{10}O_{17}:Eu^{2+}$ and AlF_3 were fired in the reduced ambience at 1600°C for 2 h.

SEM micrographs were taken of the products produced by using the mixtures of $BaMgAl_{10}O_{17}:Eu^{2+}$ and AlF_3 in various ratios (Fig. 1). The SEM results clearly indicate that the particle size of the products increases with an increase in the ratio of AlF_3. Simple firing of $BaMgAl_{10}O_{17}:Eu^{2+}$ in the absence of AlF_3 resulted in a particle size of 0.9-1.5 μm. This is the same size as that of the raw $BaMgAl_{10}O_{17}:Eu^{2+}$ phosphor used in this experiment. The particle size of the products increased linearly while increasing the ratio of AlF_3 up to 3 mol then tended to saturate over 3 mol. When the ratio of AlF_3 was 3 mol products having a particle size of 20-50 μm were obtained. This size was more than an order of magnitude larger than that of the raw $BaMgAl_{10}O_{17}:Eu^{2+}$.

The XRD patterns of the products are shown in Fig. 2. The results show that the products were almost completely $BaMgAl_{10}O_{17}:Eu^{2+}$, although a small amount of Al_2O_3 tended to be included in the products having an increased ratio of AlF_3. The results also show that XRD intensity from the crystal plane having oriented in the direction of the c-axis of $BaMgAl_{10}O_{17}:Eu^{2+}$ became stronger with an increased ratio of AlF_3. The change in XRD patterns can be explained in terms of a change in particle shape resulting from an increased ratio of AlF_3. An increased ratio of AlF_3 produced $BaMgAl_{10}O_{17}:Eu^{2+}$ having a more thin-walled, platelike, and hexagonal particle shape. The c axis of $BaMgAl_{10}O_{17}:Eu^{2+}$ having a hexagonal crystal structure is in the vertical center line of the hexagonal platelike particle. Such phenomena

Downloaded on 2016-05-09 to IP 130.203.136.75 address. Redistribution subject to ECS terms of use (see ecsdl.org/site/terms_use) unless CC License in place (see abstract).